Bioactive materials: In vitro investigation of different mechanisms of hydroxyapatite precipitation

Acta Biomaterialia 102 (2020) 468–480

Contents lists available at ScienceDirect

Acta Biomaterialia

journal homepage: www.elsevier.com/locate/actbio

Full length article

Bioactive materials: *In vitro* investigation of different mechanisms of hydroxyapatite precipitation

S. Ferraris[a], S. Yamaguchi[b], N. Barbani[c], M. Cazzola[a], C. Cristallini[d], M. Miola[a], E. Vernè[a], S. Spriano[a,*]

[a] Politecnico di Torino, Corso Duca degli Abruzzi 24, Corso Duca degli Abruzzi 24, 10129 Torino Italy
[b] Chubu University, 1200 Matsumoto cho, Kasugai Japan
[c] University of Pisa, DICI – Largo Lucio Lazzarino 1, 56126 Pisa Italy
[d] CNR, IPCF - Largo Lucio Lazzarino 1, 56126 Pisa Italy

ARTICLE INFO

Article history:
Received 24 July 2019
Revised 31 October 2019
Accepted 11 November 2019
Available online 14 November 2019

Keywords:
Bioactivity
Mechanism
Kinetics
Ti alloy
Bioactive glasses
Hydroxyapatite

ABSTRACT

Bioactive materials, able to induce hydroxyapatite precipitation in contact with body fluids, are of great interest for their bone bonding capacity. . The aim of this paper is to compare bioactive materials with different surface features to verify the mechanisms of action and the relationship with kinetics and type of precipitated hydroxyapatite over time. Four different surface treatments for Ti/Ti6Al4V alloy and a bioactive glass were selected and a different mechanism of bioactivity is supposed for each of them. Apart from the conventional techniques (FESEM, XPS and EDX), less common characterizations (zeta potential measurements on solid surfaces and FTIR chemical imaging) were applied. The results suggest that the OH groups on the surface have several effects: the total number of the OH groups mainly affects hydrophilicity of surfaces, while the isoelectric points, surface charge and ions attraction mainly depend on OH acidic/basic strength. Kinetics of hydroxyapatite precipitation is faster when it involves a mechanism of ion exchange while it is slower when it is due to electrostatic effects . The electrostatic effect cooperates with ion exchange and it speeds up kinetics of hydroxyapatite precipitation. Different bioactive surfaces are able to differently induce precipitation of type A and B of hydroxyapatite, as well as different degrees of crystallinity and carbonation.

Statement of significance

The bone is made of a ceramic phase (a specific type of hydroxyapatite), a network of collagen fibers and the biological tissue. A strong bond of an orthopedic or dental implant with the bone is achieved by bioactive materials where precipitation and growth of hydroxyapatite occurs on the implant surface starting from the ions in the physiological fluids. Several bioactive materials are already known and used, but their mechanism of action is not completely known and the type of precipitated hydroxyapatite not fully investigated. In this work, bioactive titanium and bioglass surfaces are compared through conventional and innovative methodologies. Different mechanisms of bioactivity are identified, with different kinetics and the materials are able to induce precipitation of different types of hydroxyapatite, with different degree of crystallinity and carbonation.

1. Introduction

Bioactive materials, intended as able to induce hydroxyapatite precipitation in contact with body fluids, were widely investigated as materials for bone regeneration. Their mechanism of bone bonding is based on the formation of a surface layer of hydroxycarbonate apatite (HCA), which mimics the chemical and crystallographic characteristics of bone, which is almost two-thirds made by hydroxyapatite. Bioactivity, in terms of apatite formation ability, is usually verified *in vitro* through immersion in Simulated Body Fluid (SBF) [1] that means in absence of proteins and cells, while

* Corresponding author.
E-mail address: silvia.spriano@polito.it (S. Spriano).

https://doi.org/10.1016/j.actbio.2019.11.024

bone-bonding ability needs to be proved through in vivo models. Zadpoor reviewed relationship between apatite formation in SBF and *in vivo* bone bonding [2] and it appeared that about 3/4 of the *in vitro* studies of apatite-forming ability successfully predicted *in vivo* performance of the same materials. Adsorption of growth factors and adhesion proteins (fibronectin, vitronectin etc.), which concur to the formation of the hydroxyapatite layer, the biological mechanism of bonding to bone. Besides this, the interaction of a bioactive material with physiological fluids and tissues can result in several benefits, enhancing revascularization, osteoblast adhesion, enzyme activity and differentiation of mesenchymal stem cells [3]: this is why a great effort has been made in developing bioactive glasses and titanium surfaces even through complex surface treatments.

Currently, both bioactive glasses and surface-treated bioactive titanium (or titanium alloys) are clinically used as bioactive bulk materials or as fillers and coatings within composite structures. Silicate bioactive glasses are based on the original glass developed by Larry Hench (Bioglass® [4]). Their bioactivity mechanism consists of five steps observable *in vitro*. In the first step, cation exchange from the glass network modifiers (Na^+ and Ca^{2+}) and H_3O^+ from body fluid occurs, which leaves a poorly connected silica rich layer (formation of silanol groups and silica gel layer 1-2 μm thick). This process results in an increase of the pH of the solution due to the increasing number of the OH^- ions that is dependent on the glass composition. Then, amorphous calcium hydroxyl phosphate precipitates on the silica rich layer (calcium ions precipitation followed by incorporation of the OH^-/PO_4^{3-} anions from the supersaturated solution) and crystallizes to form calcium-deficient HCA [5,6]. Hydroxyapatite formation is highly dependent on the bioactive glass composition. The different compositions developed are able to release soluble ions (Si, Ca, P and Na) to different extent from the glass surface and this affects bioactivity mechanism, kinetics, intracellular and extracellular response. Moreover, the properties of bioactive glasses have been modified by doping with elements such as Cu, Zn, In, Ba, La, Y, Fe, Cr, and Sr [7,8]. Currently, BonAlive® bioactive glass S53P4, TheraGlass), 45S5 Bioglass® (commercially developed under the trade name of PerioGlas® by NovaBone), Cerabone®, Ceravital® are among the most common bioactive glasses that reached commercial success [9]. The bioactive glass selected for this work is a state-of-the-art silica-based glass obtained by melt and quenching route. Its composition belongs to the class of 45S5 Bioglass®, modified for the different proportion between the network former and modifier oxides, as well as for the addition of small amount of B_2O_3 and Al_2O_3 to regulate reactivity, as reported in previous works [9,10,11].

Following the development of bioactive glasses, surface chemical treatments on Ti and Ti alloys were developed in order to induce bioactive behavior on a metal surface. Several chemical and heat treatments were applied to c.p. Ti and Ti-6Al-4V alloy and described in the literature [12,13]. Bioactivity of some of these materials ((NaOH-heat or NaOH-$CaCl_2$-heat-water treatments) is based on ion release and exchange with body fluids, while in other cases (NaOH-HCl-heat and HF-H_2O_2) it is based on electrostatic ion attraction.

Several properties of biological hydroxyapatite are of interest, as comparison with HCA formed on bioactive materials [3]: the low crystallinity, the crystal size smaller than 500 Å, the calcium deficiency structure, the non-stoichiometric phases, the large number of lattice defects and the micro-stresses in the network due to the presence of the carbonate groups. These stresses and defects play a vital role in the solubility of hydroxyapatite. Biological hydroxyapatites are known as type B where carbonates substitute PO_4^{3-} as a result of dissolved CO_2 in the aqueous phosphate solution. On the other side, synthetic hydroxyapatites are known as type A where the carbonate ions substitute the OH^- groups. Stoichiometry, acidity and solubility of hydroxyapatites can be evaluated through the Ca/P ratio. Higher Ca/P ratio yields lower acidity and solubility and vice versa.

The aim of this research work is to compare the formation and development over time of the HCA layer on a bioactive glass and four different metal bioactive materials, which act through different mechanisms, during *in vitro* soaking. The use of less common investigation techniques, such as the bulk zeta potential measurements (through electro-kinetic and electro-osmosis tests) and FTIR chemical imaging were adopted in addition to the usual analyses.

2. Materials and methods

2.1. Sample preparation

1.1.1. Glass synthesis

A bioactive glass (BG) with the following molar composition: 48% SiO_2, 18% Na_2O, 30% CaO, 3% P_2O_5, 0.43% B_2O_3, 0.57% Al_2O_3 was synthesized by means of the melt and quenching technique. The preparation process of the glass has already been described [10] and it is here briefly summarised. The reactants were mechanically mixed and melted in a platinum crucible at 1450 °C for 1 h. Afterward, the melt was cooled in a brass mould to obtain glass bars, which were annealed at 500 °C for 13 h and cut in slices of about 10x10x1,5 mm. Samples 13 ×33 × 1 mm were prepared for the electro-osmosis measurement of the zeta potential (see 2.3.3). All the slices were then polished with SiC abrasive papers up to 1200 grit.

1.1.2. Surface Treatments of Ti and Ti-6Al-4V alloy

Pure Ti (ISO5832-2, Nilaco Co., Tokyo, Japan) and Ti-6Al-4V alloy (ASTM B348, Gr5Titanium Consulting and Trading, Buccinasco, Italy) were cut into 10× 10 × 1 mm plates and abraded with #400 diamond plates, washed with acetone, 2-propanol and ultrapure water in an ultrasonic cleaner for a period of 30 min, then dried at 40 °C. The Ti and Ti-6Al-4V alloy samples were subjected to the chemical and heat treatments according to previous reports [13,14,15]. Briefly, Ti was soaked in a 5 M NaOH alkali solution at 60 °C, and subsequently in 50 mM HCl, then heat treated at 600 °C (denoted as Ti(A-HC-H). Some of Ti-6Al-4V alloy were soaked in the same NaOH solution at 95°C, and subjected to the same heat treatment (denoted as Ti64(A-H), or soaked in a 100 mM $CaCl_2$ solution at 40 °C after the alkali treatment followed by the heat and water treatment at 80 °C (denoted as Ti64(A-Ca-H-W). Other Ti-6Al-4V alloy were as first surface etched in hydrofluoric acid to remove the native oxide layer and then treated by controlled oxidation in hydrogen peroxide (denoted as Ti64(HF-H_2O_2). Samples 13 ×33 × 1 mm were prepared for the electro-osmosis measurement of the zeta potential (see 2.3.3); an increased volume of the etching solutions was used proportionally to the surface area to be treated.

2.2. Soaking in SBF

The samples (glass or titanium slices) were subjected to *in vitro* bioactivity test by soaking them in 25 ml of simulated body fluid (SBF-Kokubo [1]) maintained at 37 °C for 30 minutes, 1 and 3 days. The pH value of the solutions was monitored during SBF immersion. In the case of the glass, the pH changes from 7.4 to 7.7 (±0.02) after 3 days. In the case of all the Ti and Ti6Al4V samples, the pH remains in the 7.4-7.5 range for the whole soaking time.

After soaking, the samples were washed under a gentle flow of ultrapure water (500 ml per sample) in order to remove the residual SBF compounds :

2.3. Surface analysis

2.3.1. Scanning electron microscopy (FE-SEM) and energy dispersive X-ray analysis (EDX)

The Ti and Ti alloy samples subjected to chemical and heat treatments and the bioactive glass samples were observed both through top and cross-sectional observations; the samples for cross-sectional observation were broken by bending. The samples were coated with a Pt–Pd thin film, then observed under field emission scanning electron microscopy (FE-SEM: S-4300,Hitachi Co., Tokyo, Japan) with a voltage of 15 kV. EDX analysis was performed by an energy dispersive X-ray spectrometer (EDX: EMAX-7000, Horiba Ltd., Kyoto, Japan) by using 9 kV with the resolution of approximately 1 μm in spot size on the samples that have been soaked in SBF for 3 days (in order to investigate nucleation and evolution of hydroxyapatite) and subjected to carbon coating.

2.3.2. X-ray photoelectron spectroscopy (XPS)

The elemental surface chemical composition of the samples (one per type) was analyzed by using X-ray photoelectron spectroscopy (XPS, PHI 5000 Versaprobe II, ULVAC-PHI, Inc., Kanagawa, Japan). The XPS take-off angle was fixed at 45 degrees so that photoelectrons to a depth of 1 to 5 nm from the surface are able to be detected. An Al-K radiation line with energy resolution of below 0.5 eV was used as the X-ray source with step interval of 0.1 eV. The calibration of the measured spectra was performed by reference to the C1s peak of the surfactant CH_2 groups on the substrate occurring at 284.8 eV in binding energy.

2.3.3. Zeta potential measurements

An electro-kinetic analyzer (SurPASS, Anton Paar) has been employed for the zeta potential titration vs pH. The surface zeta potential was determined in function of the pH in a 0.001 M KCl electrolyte solution varying the solution pH by addition of 0.05M HCl or 0.05M NaOH through the instrument automatic titration unit. The acid and alkaline sides of the curve were obtained in two different steps on the same set of samples or on a different one, depending on the surface reactivity, as discussed in the following. For each pH value, 4 measurements were taken and an average value reported with its standard deviation. The zeta potential was also monitored as a function of time at the constant pH value of 7.4, in this case diluted SBF (dropwise addition of SBF in water up to the reaching of a pH value equal to 7.4 and at about 15 mS/m) was used as electrolyte. 4 measurements were taken for each time point and an average value was reported with its standard deviation.

The zeta potential was also measured through an electro-osmosis method. Samples were set in a glass cell of a zeta potential and particle size analyzer (model ELS-Z1, Otsuka Electronics Co., Japan). The glass cell was filled with a 1 ml of a 10 mM NaCl solution dispersed with monitoring particles of polystyrene latex (size = 500 nm) that are coated by hydroxyl propyl cellulose. The zeta potentials of the samples were measured under an applied voltage of 40 V. The measurement was repeated on five different samples and the averaged values were used. The measurements on Ti64 alloys were incapable because of high electrical conductive feature of the surfaces formed on the alloys. The leak of electric current was confirmed by comparing an electrical resistance of the system (cell constant) with the alloy samples to that obtained with a platinum plate which is an electrical conductive material due to lack of a native oxides on its surface. The cell constants of the system with the alloy samples were found to be around 30: this value is close to 27 which is the value obtained with the platinum plate. This indicates that the electric current leaked off through the alloy substrates. In contrast, the cell constants of the system with the treated cp-Ti and bioactive glass samples were 58 and 66, respectively: this indicates a little or almost no leak of electric current during the measurements. The high electrical conductivity of the alloy surfaces is probably due to the alloying elements such as V. It is well known that titanium oxides are electrical insulating, but increase their electrical conductivity by the presence of traces of metal ions [16,17].

2.3.4. Fourier Transform Infrared Spectroscopy

Spectral images were carried out by means of a Perkin Elmer Spectrum Spotlight 300 FT-IR Imaging System, using the “point” mode of the instrument. For each sample, an area of 1 mm × 1 mm was analysed and an IR image was produced using a liquid nitrogen cooled, 16-pixel mercury cadmium telluride (MCT-A) line detector. An absorbance spectrum was recorded for each pixel in the μATR mode. The specific areas of interest were identified by means of the optical microscope, the ATR objective (Ge, less than 1 μm depth) was touched on the sample, the spectra generated from the surface layers of the sample were collected, and IR spectral images were produced. The spotlight software (PerkinElmer, Norwalk, CT) used for the acquisition was also used to pre-process the spectra. All spectra were recorded in the mid infrared region (4000–750 cm^{-1}) at 16 scans per pixel; the spectral resolution was 4 cm^{-1}; the spatial resolution was 100 × 100 μm. The recorded spectral maps were elaborated using the software of the instrument to obtain a correlation map and a band absorbance ratio. The acquired chemical map was used to obtain the average spectrum, which is the most representative spectrum of the chemical map. Band ratio analysis is commonly used for quantification in infrared spectroscopy. This involves the measurement of either the peak absorbance or the band area of an internal reference, with respect to the corresponding values of a band of interest. In the present paper, ratio band between a carbonate contribution (numerator, 1635–1335 cm^{-1}) and a phosphate contribution (denominator, 1171-901 cm^{-1}) was measured to evaluate the degree of carbonation by using an area-based method [18].

2.4. Statistical analysis

All the data from FE-SEM pictures, such as measurements of pore sizes and thickness of the oxide layers, were performed by averaging 15 measurements for each specimen.

Concerning FTIR chemical imaging, a statistical analysis was performed by Principal Component Analysis (PCA). This is a powerful method for the analysis of large spectral data sets. It represents the spectra in data groupings of similar multi-parameter variability and allows the identification and differentiation of dissimilar spectral groups, such as e.g. data sets corresponding to different samples or regions of samples. The scatter plots were exploited to identify the clusters of data more significantly associated to hydroxyapatite deposition. The Spotlight software was used to evaluate the presence and distribution of the different components and to obtain the chemical and correlation maps.

3. Results

The features of the as-prepared surfaces were characterized and compared: the data are reported in Sections 3.1–3.4. The surface features of the investigated materials are summarized in Table 1 for a better comparison and easier correlation to their properties.

Nucleation of hydroxyapatite was investigated during the first 30 min of soaking in SBF by measurement of the electro-kinetic zeta potential vs time at the physiological pH in a diluted SBF solution (Section 3.5) and after 30 min of soaking by FTIR chemical imaging analysis (Section 3.6) and XPS (Section 3.7). The hydroxyapatite further evolution was analyzed after 1 day of soaking (the

Table 1
Summary of the surface features of the investigated materials.

	Morphology	Thickness of the oxide layer [micron]	Characteristic element(s) on the surface	Surface chemistry					IE	Hydrophilicity
				O^{2-} [%]	$(OH)_a$		$(OH)_b$			
Ti(A-HC-H)	Nanoporous (larger than 200 nm)	1.2-1.6	-	91	2%	weak	7%	strong	5.6 Affected by strong $(OH)_b$	+
Ti64(A-H)			Na	85	11%	Not specific	4%	very weak	3.5 Limited effect of $(OH)_a$	+
Ti64(A-Ca-H-W)			Ca	77	20%	very weak	3%	very weak	3.8 Not affected by $(OH)_{a,b}$	++ Affected by the high total amount of OH
Ti64(HF-H_2O_2)	Nanoporous (100 nm)	0.4	-	30	56%	strong	14%	weak	2 Affected by strong $(OH)_a$	++ Affected by the high total amount of OH
BG	Flat	-	Ca/Na	90	10% (strong acidic + weak basic)				3.1 Affected by strong $(OH)_a$	+

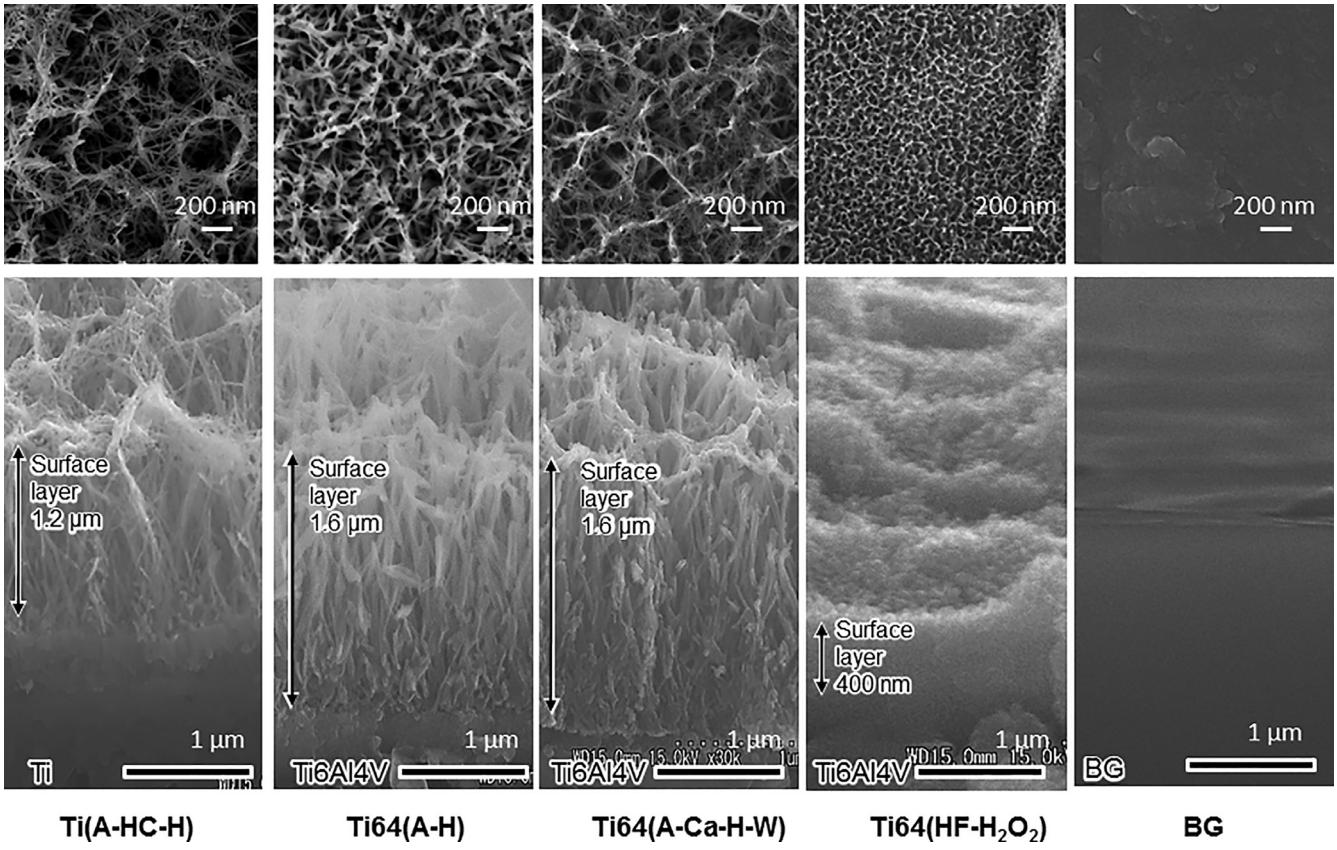

Fig. 1. FE-SEM top (a) and cross-sectional (b) view of the as-prepared samples.

FTIR and XPS data are reported in Sections 3.6-3.7) and 3 days of soaking (the FE-SEM and EDX data are reported the in Section 3.8).

3.1. Morphology of the surface of the as prepared samples

All the Ti based treated surfaces are characterized by a surface layer with a porous morphology on the nanoscale while the glass has a smooth surface (Fig. 1a – top view of the samples). Porosity of Ti64(HF-H_2O_2) is on a smaller scale than the other Ti based treated surfaces, with an average pore diameter lower than 100 nm instead of 100-200 nm in the case of Ti64(A-H) and higher than 200 nm in the case of Ti(A-HC-H) and Ti64(A-Ca-H-W)).

The thickness of the surface treated layer (Fig. 1b – cross-sectional view of the samples) is below 500 nm in the case of Ti64(HF-H_2O_2), which is only chemically treated, while it is above 1 micron for the other Ti samples which are both chemically and heat treated (Ti(A-HC-H) – Ti64(AH)-Ti64(A-Ca-H-W)). The morphology of the surface layers across the thickness is highly porous and shaped like filaments in the case of Ti64(A-H), Ti(A-HC-H) and Ti64(A-Ca-H-W), while it is much more dense on Ti64(HF-H_2O_2).

3.2. XPS analysis of the as prepared samples

Fig. 2a shows the results of the XPS quantitative analysis on the as-prepared samples.

As expected, the oxide layer of Ti(A-HC-H) and Ti64(HF-H_2O_2) is only composed of Ti and O, whereas Ti64(A-H) and Ti64(A-Ca-H-W) contain some amount of Na and Ca, respectively. It should be noted that some amount of the alloying elements (Al and V) were detected on Ti64(A-H) and Ti64(A-Ca-H-W) and a larger amount of Al was detected on Ti64(HF-H_2O_2).

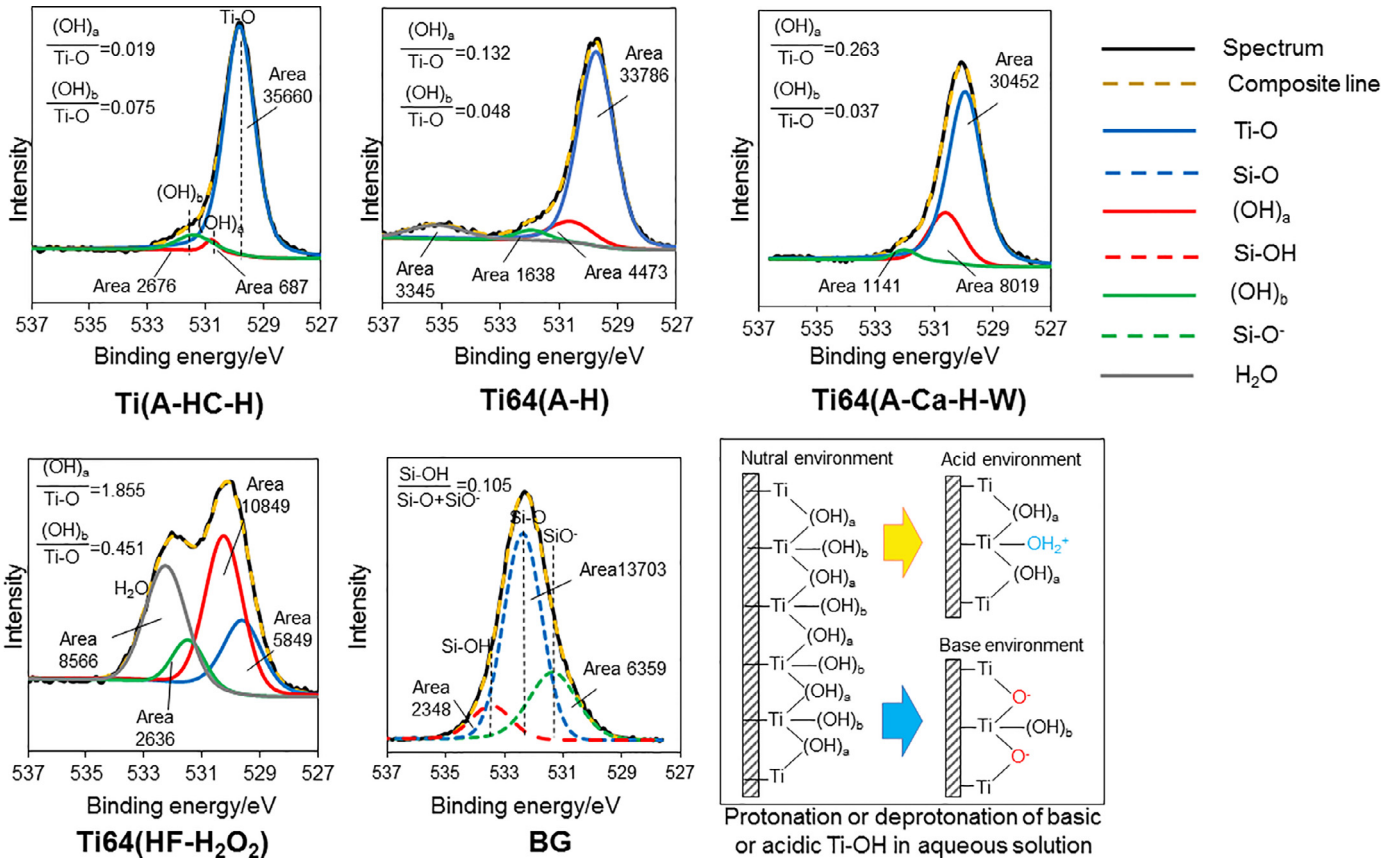

Fig. 2. XPS data of the as-prepared surfaces. (a) surface composition from survey spectra; (b) fitting profile of the oxygen region; - means not measured.

In the case of BG, the elements are detected in a ratio matching the nominal glass composition; B is present in the glass, but its amount cannot be exactly evaluated by XPS and it is not reported.

The profile analysis of the O1s signals is shown in Fig. 2b.

In the case of the Ti based materials, the oxygen signal can be decomposed into three contributions around 530, 531 and 532 eV which are respectively attributed to Ti-O, the acidic Ti-OH groups (denoted as $(OH)_a$) and the basic Ti-OH groups (denoted as $(OH)_b$) [19]. The $(OH)_a$ groups are bridging and they become negatively charged by releasing H^+ in basic aqueous solutions, while the $(OH)_b$ are terminal groups and they become positively charged by accepting H^+ in acidic aqueous solutions as shown in Fig. 2 (right corner) [20].

On Ti(A-HC-H), the $(OH)_a$/Ti-O ratio is 0.019 and it is significantly lower than the $(OH)_b$/Ti-O ratio (that is 0.075): a prevalence of the basic OH groups with respect to the acidic ones characterizes this surface. In contrast, $(OH)_a$/Ti-O becomes greater on Ti64(A-H), Ti64(A-Ca-H-W) and Ti64(HF-H_2O_2): respectively: 0.132, 0.263, 1.855.

In the case of BG, three contributions to the oxygen peak are found according to the literature [21]: two related to the oxide and one to the OH groups. The ratio of Si-OH to oxide (Si-O and SiO^-) was found to be 0.105 on BG.

These data are summarized as percentage values in Table 1.

3.3. Electro-kinetic titration curves of the as prepared surface layers

The titration curves (Fig. 3) are obtained by testing as first the basic range and then the acidic one, starting in both cases from pH 5.5. The point of boundary between the basic and acidic ranges of each curve (that is the starting point of the two measurements) is marked on the figure: a significant step of the curve at this point (higher than 15 mV), as well as high standard deviation of the zeta potential in the curve (higher than 0.5-1 mV as usually registered) evidence that the material is not stable during the measurement and some reactions occurred. No relevant step and unusual standard deviation was observed in the case of the Ti based treated surfaces: the oxide layer has in all cases a passive behavior and good resistance to corrosion. On the other side, it was observed in the case of BG and untreated Ti6Al4V an increased standard deviation (3-4 mV) in the basic range due to the reactivity of these materials in the basic environment. In these cases, the reported curves were obtained by using different sets of specimens for the acidic and basic ranges in order to test in both the ranges the as-prepared surface. The reported curve of BG evidences the reactivity of the material at a pH higher than 8 with a change in the slope of the curve.

The isoelectric point of a surface is related to the balance between the functional groups with acidic and/or basic behavior in contact with a solution; it is around 3.7-4.1 for the untreated Ti and Ti6Al4V alloy, which is what expected for surfaces almost free from charged functional groups or with a balanced effect of them.

The isoelectric point moves to a higher pH value in the case of the Ti(A-HC-H) sample (IE = 5.6), proving the prevalence of basic functional groups on this treated surface; this is in agreement with XPS data where a prevalence of the basic OH groups on the acidic ones was detected. The effect of the relative number of the OH groups with respect to the O^{2-} specie will be discussed in the following.

On the contrary, the isoelectric point is shifted toward a lower pH value in the case of Ti64(HF-H_2O_2) (IE≈2), revealing the prevalence of the acidic groups on this surface, in agreement with the XPS data. In this case, the IE value must be obtained by interpolation because the instrument cannot reach such a low pH value.

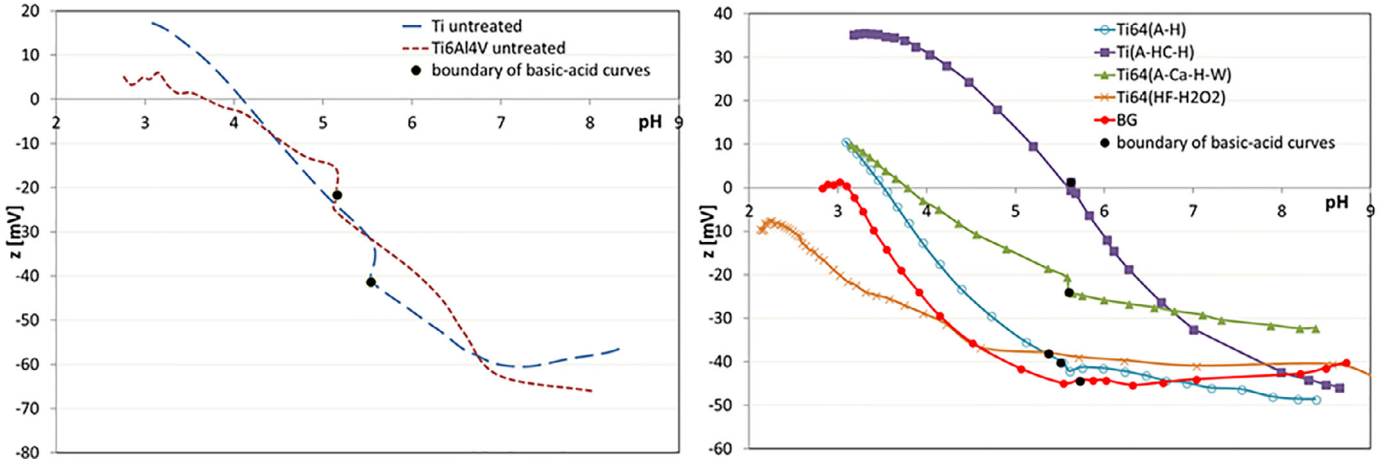

Fig. 3. Electro-kinetic zeta potential titration curves of the as-prepared surfaces; the curves of the un-treated Ti and Ti6Al4V alloy are reported as reference.

Similarly, BG has a low value of IP (IE = 3.1) revealing the acidic character of the OH groups detected by XPS. As last, a similar effect, occurs on Ti64(A-H), but the shift toward the acid values of the IE is lower (IE = 3.5).

The isoelectric point of the Ti64(A-Ca-H-W) sample does not significantly change with respect to the un-treated substrate (IE = 3.8), even if a significant number of OH groups (mainly acidic) was detected by XPS on these samples: the explanation of this effect will be discussed later.

Looking at the shape of the titration curves, Ti64(HF-H_2O_2) clearly has a plateau in the basic range with onset at pH 4.5. This phenomenon reveals that all the acidic OH groups on this material act like an acid with a specific acidic strength; considering that the onset of the plateau is the minimum pH value at which they are completely deprotonated, that is a significantly low value in this case, the acidic OH groups on this surface act as a strong acid.

Similarly, BG has a plateau with onset at pH = 5.5. It can be deduced that even if these groups are in low number on the surface (XPS data) they have a great effect on the surface charge of the material (according to the significant shift of the IE) because of their strong acidic strength. BG and Ti64(HF-H_2O_2) show also a plateau at the very low pH values: this is related to the presence of the basic OH groups with a weak basic strength (detectable only at very low pH).

The curve of the sample Ti64(A-H) has a change of slope around pH 5.5, but in this case a real plateau with a constant zeta potential value is not reached. It can be supposed that some OH groups with high acidic strength are present, but actually they have not a specific acidic strength, so they are not completely deprotonated at the same pH value. This explanation is in agreement with the previously reported low effect on IE.

Ti(A-HC-H) clearly evidences the presence of a single type of basic functional groups with an evident plateau in the acidic range: the surface has a positive surface charge at a pH lower than 5.6 and all the basic functional groups are completely protonated at a pH lower than 3.5, with a strong basic behavior. Again, the strong chemical behavior of these basic groups can explain the shift of the IE of this surface even if they are in a low number (XPS data). This behavior is in agreement with the consistent presence of anatase on this surface [14]: pure anatase, in fact, has an IE point higher than rutile (6.2 with respect to 5.3) with a prevalence of the basic OH groups [22]. On the other side, no effective plateau is observed in the acidic range, even if a change of slope is observed, probably because the acidic OH groups are weak and without a single specific acidic strength on this surface.

The curve of Ti64(A-Ca-H-W) shows and almost linear trend without any evident plateau: it means that even if the functional groups are exposed on the surface (as evidenced by XPS), they are too weak to react within the explored pH range and this explain the absence of an effect on the IE value.

It can be observed that Ti64(HF-H_2O_2) and Ti64(A-Ca-H-W) have a lower slope of the curves than the other materials: this effect is related to surface hydrophilicity as discussed in Section 4.

3.4. Electro-osmosis zeta potential measurements of the as prepared surface layers

The electro-osmosis zeta potential measurements were performed in order to get complementary information at the physiological pH. In fact, the electro-kinetic technique makes measurements with a consistent flux of fluid (600 ml), while electro-osmosis measurement is made in presence of a fluid micro-environment (1 ml) at the physiological pH (7.0-7.4).

Ti(A-HC-H) showed positive surface charge under this condition (+8.5 mV).

The zeta potential of BG was measured as -17.8 mV that is a less negative value than that of the electro-kinetic zeta potential measurement confirming that this type of measurement is affected by local release of ions and the results of these two techniques cannot be directly compared.

As explained in the Materials section, the measurements on Ti64 alloys were incapable, but in these cases no specific surface charge difference was expected in a microenvironment, as discussed in section 4.

3.5. Electro-kinetic zeta potential vs time at the physiological pH (diluted SBF solution)

Nucleation of hydroxyapatite can be monitored by following the change in surface charge during the first minutes of soaking in SBF, this is the reason why the electro-kinetic zeta potential was measured vs time in a diluted SBF solution for 30 min (Fig. 4). A constant lowering of the zeta potential of about 5 mV with respect to the values registered at pH 7.4 in diluted KCl is observed for all the curves. This effect was observed also on a Ti sample coated by a thin Pt film used as a model of an inert surface (un-reported data) and is related to the different ionic strength of the solutions.

An evident shift of the zeta potential toward less negative values (+17 mV) occurs during the test on BG, evidencing the high reactivity and fast ion exchange of this material. The increment

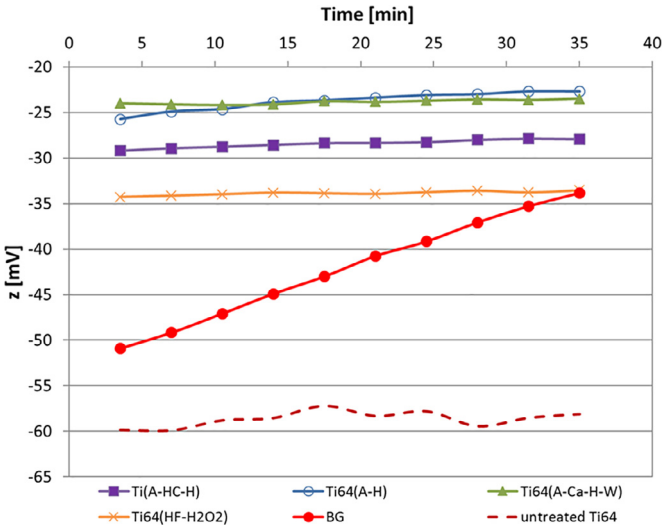

Fig. 4. Electro-kinetic zeta potential vs time curves of the samples during soaking in diluted SBF solution.

of the surface charge can be explained by considering the release of Na^+ ions and adsorption of Ca^{2+} ions from SBF. In this case, a slight increment of the pH (+0.4) was also observed during the measurements according to adsorption of H_3O^+ ions on the surface.

The Ti based treated surfaces show a higher surface charge with respect to the untreated substrate according to the formation of an oxide layer during the surface treatments, but no evident increment is observed during the measurement. Only, Ti64(A-H) shows a slight increment (+3 mV) of the zeta potential according to the ion exchange mechanism close to that of BG (release of Na^+).

3.6. FTIR chemical imaging analysis

FTIR Chemical Imaging analysis was performed on the different materials in order to investigate the nucleation (after 30 min of soaking in SBF) and first evolution (after 1 day of soaking in SBF) of apatite. The as-prepared surfaces for all samples were analyzed as reference and all data are reported in this section for a better comparison (Fig. 5 a–k).

The spectra acquired from the surfaces of the Ti-based materials showed a band at 1190 cm^{-1} assigned to the Ti-O bonds [23]. The as-prepared Ti(A-HC-H), Ti64(A-Ca-H-W) and Ti64(HF-H_2O_2) samples showed a chemical image characterized by a broad band in the range 3500-3300 cm^{-1} associated to the OH stretching vibration frequency [24]. This band appeared particularly intense in the Ti64(HF-H_2O_2) sample indicating the presence of the hydroxyl groups and water molecules on the surface. The presence of water was also confirmed by the peak at 1630–1640 cm^{-1} that can be assigned to the H-O-H bending vibrations of water as well as of Ti-OH.

Concerning the as-prepared BG sample, the characteristic peak of the chemical map showed a band at 896 cm^{-1} with a shoulder at 993 cm^{-1} due to Si-O bonds and two weak absorption bands at 1605 cm^{-1} and 1423 cm^{-1} attributable to the presence of an amorphous phase (Fig. 5e).

In the spectra of the Ti64(A-H) (Fig. 5a) and BG (Fig. 5e) samples, it is evident a small peak at about 900 cm^{-1} due to the stretching vibration of the Ti-O bonds involving a non-bridging oxygen coordinated with the sodium ions (results in agreement with XPS analysis [25].

The optical image of Ti64(A-H) soaked for 30 min showed the presence of an amorphous material which covered only partially the surface (Fig. 5b), the spectra acquired on this surface showed the deposition of a thin layer of carbonate (1420 cm^{-1}) and acidic phosphate (1136 cm^{-1}) (Fig. 5c). The correlation map gave values close to 1 only in some areas of the analyzed surface confirming the result of the optical image (Fig. 5d).

The optical image of BG soaked for 30 min pointed out the presence of an amorphous material on the surface (Fig. 5f). Two kinds of spectra were acquired on different points of the surface that differed in the intensity of the broad peak in the range 3000–3600 cm^{-1}; all spectra showed the presence of carbonates at 1560-1430 cm^{-1}, acidic phosphates at 1180 cm^{-1}, phosphate at 1040 cm^{-1} and silica at 895 cm^{-1} (Fig. 5g). The values of correlation map confirmed a good homogeneity of the amorphous material on the surface (Fig. 5h).

The spectra acquired from the chemical maps of Ti(A-HC-H) and Ti64(A-Ca-H-W) soaked for 30 min did not detect the presence of hydroxyapatite precursors to the titanium surface (Fig. 5i–j). Ti64(HF-H_2O_2) showed a small absorption at 1425 cm^{-1} that could indicate an early deposition of the carbonate species (Fig. 5k). These results seem to indicate that BG surface favors the deposition of HA lattice already after the first minutes of soaking in SBF, if compared to the Ti-based samples, independently from the surface treatment.

In Fig. 6 a–o, the spectra acquired from the chemical maps of the samples Ti(A-HC-H), Ti64(A-H), Ti64(A-Ca-H-W) and BG soaked for 1 day showed the characteristic bands related to adsorbed water, the phosphate and carbonate species. The correlation maps, obtained from the chemical maps, showed values close to 1 for all the surfaces analyzed indicating a good chemical homogeneity.

After 1 day of soaking, Ti(A-HC-H) appears to be covered by a homogeneous layer of apatite. The statistical analysis carried out by PCA shows a spectral variability mainly characterized by two zones that differ in the intensity of the spectra. The FT-IR spectra obtained from the chemical map showed a broad peak in the range 3000-3600 cm^{-1} corresponding to water and a peak at 1640 cm^{-1} attributed to water associated with HA. It is also present a small band at around 3700 cm^{-1} due to the OH^- ions. The bands related to the carbonate species were identified at 1480 cm^{-1}, 1455 cm^{-1} and 1413 cm^{-1} and 873 cm^{-1}. In the spectra, the typical band at about 1020 cm^{-1} due to ν_3 stretching vibration of PO_4^{3-} was also evident (Fig. 6k).

Analogously, on Ti64(A-H) soaked for 1 day, a homogeneous layer of hydroxyapatite covered the surface. The statistical analysis carried out by PCA showed a coated surface (98%), with a material having the same spectral characteristics of the Ti(A-HC-H) sample (Fig. 6g).

Also, on Ti64(A-Ca-H-W) soaked for 1 day, a layer of hydroxyapatite covered the surface. The PCA showed a spectral variability mainly characterized by two zones that differ for the spectral intensity. In this sample, it was observed the carbonate bands at 1570 cm^{-1}, 1480 cm^{-1}, 1455 cm^{-1} and 1416 cm^{-1} and also a decrease of the band at 873 cm^{-1}. The presence of an absorption band at 1480 cm^{-1} could indicate the presence of carbonate in the amorphous phase. Spectral data showed a shift of the phosphate band towards higher frequencies (1025 cm^{-1}) indicating a higher degree of crystallinity of the material (Fig. 6m). The surface of the BG sample appeared covered of hydroxyapatite. The PCA analysis allowed the identification of two areas characterized by spectral variability. The red zone (42%) showed absorption bands, related to the carbonate vibrations, at 1564-1420 cm^{-1} with two shoulders at 1480 cm^{-1} and at 1455 cm^{-1}, a small band at 873 cm^{-1} and an absorption band due to the phosphates at 1017 cm^{-1}. The green zone (57%) was characterized by a significant reduction both of the carbonate bands and of the broad band at 3000-3600 cm^{-1}. In these spectra it was observed a shift of phosphate absorption towards 1030 cm^{-1} indicating a greater crystallinity of hydroxyapatite

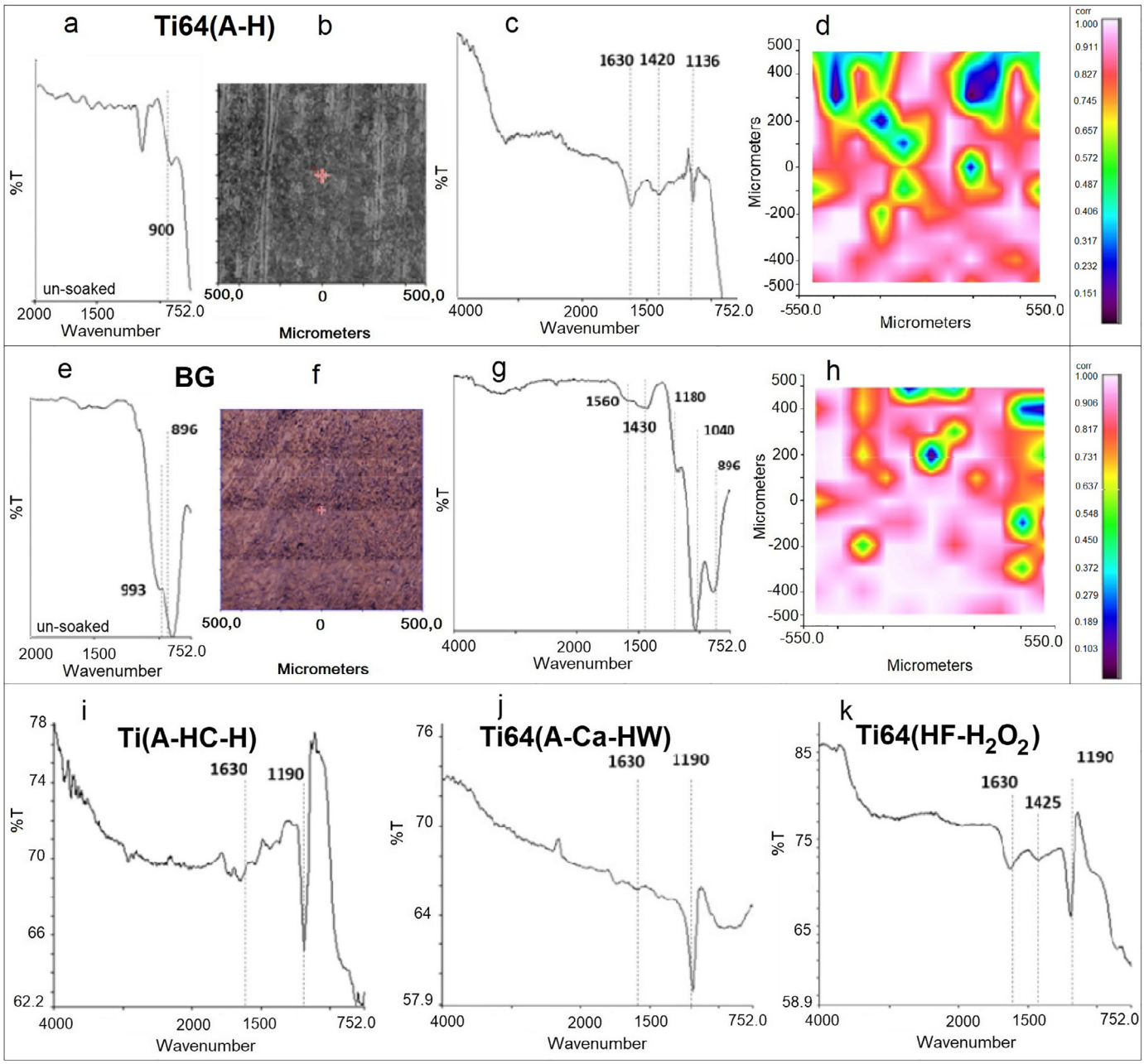

Fig. 5. FTIR Chemical Imaging. Ti64(A–H) sample (a) as-prepared (spectrum), (b–d) soaked for 30 min (optical image, spectrum, correlation map); BG sample (e) as-prepared, (f–h) soaked for 30 min (optical image, spectrum, correlation map); Ti(A-HC-H), Ti64(A-Ca-H-W) and Ti64(HF-H_2O_2) samples soaked for 30 min (i–k) (spectrum).

(Fig. 6o). In the literature, the carbonate bands, at about 1546 cm^{-1} (asymmetric stretch ν_3) and 880 (ν_3 CO_3^{2-}) cm^{-1}, can be used to identify the type A carbonate replacement (CO_3 substituting OH) while the presence of the peaks at 1415-1460 (ν_3 CO_3^{2-}) and 873 (ν_2 CO_3^{2-}) showed the formation of type B hydroxyapatite (CO_3 substituting PO_4) [26].

The spectra obtained from the chemical image of Ti64(HF-H_2O_2) soaked for 1 day showed no significant changes compared to those obtained for the other samples soaked for 30 min, except for two small absorption at 1425 cm^{-1} and 1065 cm^{-1}. This indicates a slowdown in the deposition of HA for this sample (Fig. 6n). On the basis of the carbonate band, the hydroxyapatite lattice on the surface of Ti(A-HC-H) and Ti64(A-H) can be identified as carbonated non-stoichiometric HA with prevalent replacement of type B [27]. In the samples Ti64(A-Ca-H-W) and BG, the material deposited on the surface can be identified as carbonated non-stoichiometric hydroxyapatite with replacement of type A-B.

The chemical map as a function of the band ratio was carried out in view of the carbonation quantification for the samples soaked for 1 day. The chemical maps, as a function of the band ratio, showed variability in the R values. In Table 2, R values and wt.% of carbonate for all the samples were reported.

All the maps show variability in the band ratio indicating a non-homogeneous carbonation degree at level of the sample surface. In addition, where the R value is lowest and consequently the carbonation degree is decreased, the crystallinity of HA material tends to increase, as reported in the literature [26]. The wt% of carbonate in the analyzed samples resulted from 2.4-5.8 wt%, in accordance with the values reported in the literature in a range of 3 to 8 wt% which corresponds to the carbonate content of the

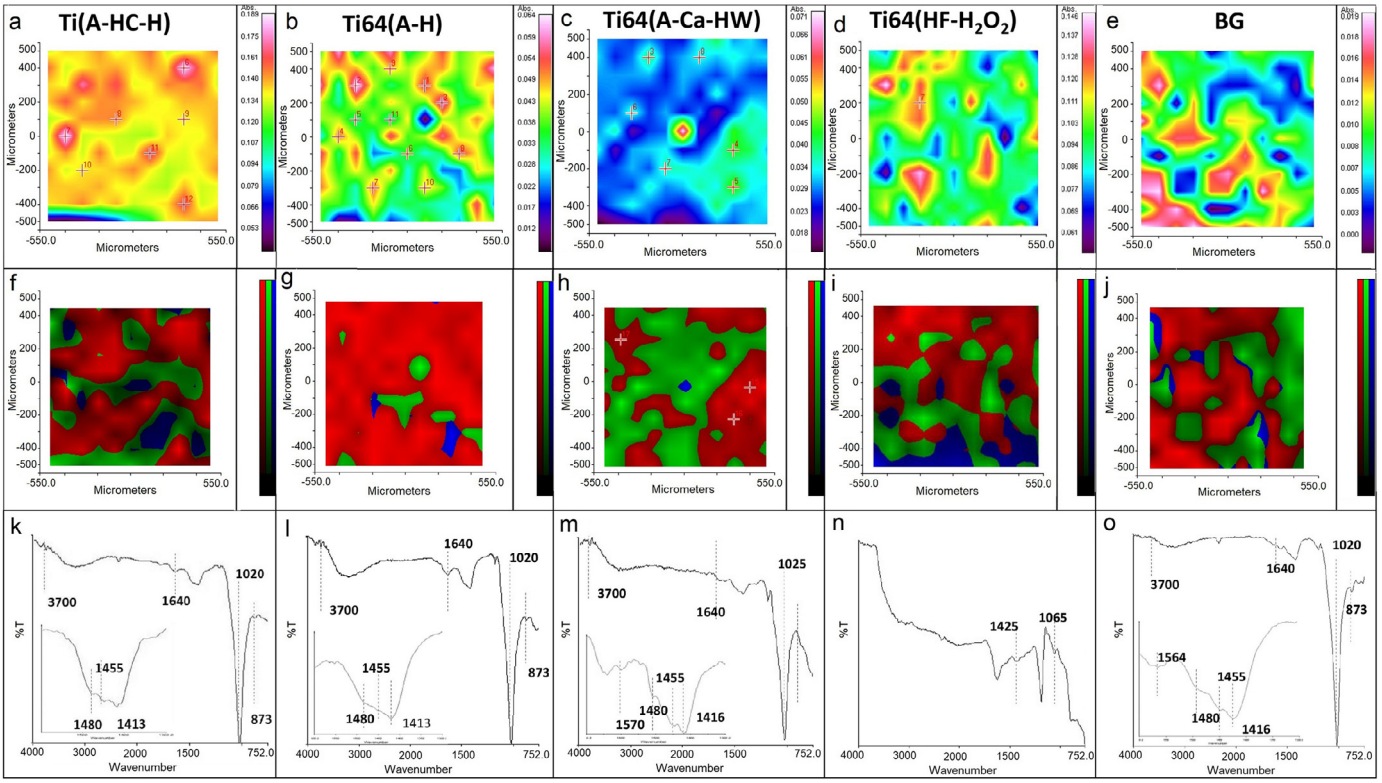

Fig. 6. FTIR chemical imaging. chemical map (a–e); PCA analysis (f–j); spectra (k–o) of Ti(A-HC-H), Ti64(A–H), Ti64(A-Ca-H-W), Ti64(HF-H2O2), BG samples soaked for 1 day, respectively. Three different scores of PCA analysis, corresponding to different percentages of the spectra data groupings of similar variability, are showed in red, green and blue colors. (For interpretation of the references to color in this figure legend, the reader is referred to the web version of this article.)

Table 2
Band ratio values between carbonates (1600–1335 cm^{-1}) and phosphates (1171–901 cm^{-1}) and weight percentage of carbonate on the samples soaked for 1 day.

Samples soaked for 1 day	Ratio band ν_3 CO_3/ ν_3 PO_4 and percentage of carbonate					
	R_{max}	wt % CO_3	ν_3 PO_4	R_{min}	wt % CO_3	ν_3 PO_4
Ti(A-HC-H)	0.13	3.8	1020 cm^{-1}	0.12	3.5	1020 cm^{-1}
Ti64(A-H)	0.19	5.5	1020 cm^{-1}	0.14	4.1	1020 cm^{-1}
Ti64(A-Ca-H-W)	0.16	4.7	1020 cm^{-1}	0.10	2.9	1025 cm^{-1}
BG	0.20	5.8	1020 cm^{-1}	0.08	2.4	1030 cm^{-1}

Table 3
XPS data of the samples after soaking. surface composition from survey spectra (soaking for 30 min and 1 day).

Sample	Element/at. %							
	O	Ti	Na	Ca	P	Al	V	Si
Ti(A-HC-H) 30min SBF	65.9	33.6	-	0.0	0.5	-	-	-
Ti(A-HC-H) 1day SBF	66.0	0.5	-	19.6	13.9	-	-	-
Ti64(A-H) 30min SBF	59.6	26.5	12.7	1.2	0.0	0.0	0.0	-
Ti64(A-H) 1day SBF	64.3	0.3	0.5	20.2	14.7	0.0	0.0	-
Ti64(A-Ca-H-W) 30min SBF	65.3	29.9	-	4.8	0.0	0.0	0.0	-
Ti64(A-Ca-H-W) 1day SBF	65.4	6.3	-	17.0	11.3	0.0	0.0	-
Ti64(HF-H_2O_2) 30min SBF	74.0	21.6	-	1.6	0.1	2.7	-	-
Ti64(HF-H_2O_2) 1day SBF	73.9	20.1	-	2.1	1.4	2.5	-	-
BG 30min SBF	69.0	-	5.0	1.4	0.3	1.5	-	22.8
BG 1day SBF	67.0	-	0.4	18.1	12.6	0.0	-	1.9

biological hydroxyapatite of most human hard tissues, with a prevalent type B substitution as well as a mixed Type A-B substitution [18].

3.7. XPS analysis of the soaked samples

Table 3 shows the XPS quantitative analysis on the samples soaked in SBF for 30 min (for investigation of hydroxyapatite nucleation) and 1 day (for investigation of hydroxyapatite first evolution).

It can be seen that phosphorous is initially enriched on the surface of Ti(A-HC-H) during the soaking (30 min), as the result of a competition with the calcium ions.

In contrast, the calcium ions were initially adsorbed on the surfaces of Ti64(A-H), Ti64(A-Ca-H-W), Ti64(HF-H_2O_2) and BG (30 min). In the case of Ti64(A-H), a progressive reduction of Na on the

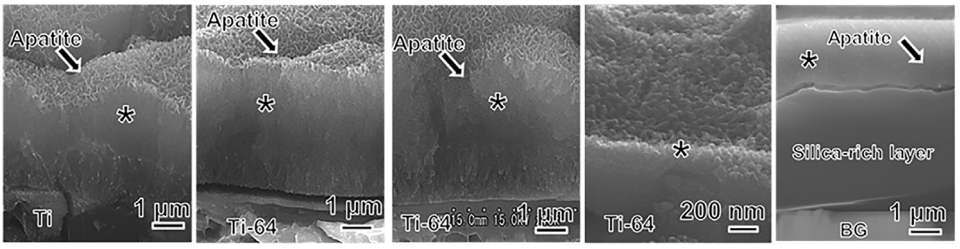

Sample	Element/at. %								
	O	Ti	Na	Mg	Ca	P	Al	V	Si
Ti(A-HC-H)	71.39	3.94	0.35	0.65	13.10	10.57	-	-	-
Ti64(A-H)	67.38	6.66	1.32	0.57	13.32	10.21	0.29	0.25	-
Ti64(A-Ca-H-W)	76.36	0.26	0.38	0.56	12.49	9.92	0.00	0.04	-
Ti64(HF-H_2O_2)	63.27	30.51	0.11	0.12	0.55	0.44	4.27	0.74	-
BG	77.01	-	0.52	0.41	12.03	8.89	0.01	0.06	1.07

b

Fig. 7. (a) Cross-sectional view of the different samples after soaking in SBF for 3 days; (b) EDX analysis of the point marked with an asterisk of the different samples after soaking in SBF for 3 days.

surface is observed moving from the as-prepared sample (Fig. 2a) to the soaked ones for 30 min and 1 day (Table 3).

After 1 day of soaking, P and Ca are detected on Ti(A-HC-H), Ti64(A-H), Ti64(A-Ca-H-W) and BG in a comparable amount and ratio (Ca/P = 1.4-1.5), while the elements of the substrates (Ti or Si) are hardly detected. A higher elemental contribution related to the substrate is detected only in the case of Ti64(A-Ca-H-W). In the case of Ti64(HF-H_2O_2), the development of calcium phosphate on the surface after 1 day of soaking is quite lower than on the other surfaces: Ca and P are present in a low amount, even if their ratio is analogous to the other surfaces, while the amount of Ti is high.

3.8. Cross-sectional observation and EDX analysis after 3 days of soaking

The further evolution of the hydroxyapatite formation on the different samples was investigated after 3 days of soaking in SBF by a cross-sectional observation of the samples and EDX analysis of their top-surface. This type of analysis was selected because XPS has not an adequate penetration depth when a thick layer of hydroxyapatite (about 1 micron) is on the surface; on the other side, EDX is not effective in order to analyze nucleation and first evolution of hydroxyapatite (such as after 1 day of soaking) because of its high penetration depth (around 1 micron below the surface). The results are reported in Fig. 7. A continuous layer of apatite, about 1 micron thick, is formed on the samples Ti(A-HC-H), Ti64(A-H),Ti64(A-Ca-H-W) and BG; the contribution to the surface elemental composition from the substrate is quite limited in all these cases. On the other side, Ca and P are detected by EDX on Ti64(HF-H_2O_2), but a layer of hydroxyapatite cannot be observed. On BG, a layer of silica gel about 10 μm thick is also observed below apatite, as expected.

4. Discussion

Different bioactive materials are investigated in this research work in order to compare the hydroxyapatite nucleation and evolution on materials with different surface features and to verify the supposed mechanisms of bioactivity.

Ti was used as a substrate in the case of Ti(A-HC-H) while Ti6Al4V was used for Ti64(A-H), Ti64(A-Ca-H-W) and Ti64(HF-H_2O_2) according to the literature [13–15]. The use of different substrates is due to their different corrosion resistance which affects the ability to form titanium oxide layers through the different chemical etching procedures. Once the titanium oxide layers are formed, the mechanism of hydroxyapatite precipitation is not related to the type of substrate and this difference does not affect the comparison.

In the case of Ti(A-HC-H) and Ti64(HF-H_2O_2), the bioactivity mechanism is supposed to be based on the presence of a specific surface charge (that is respectively positive and negative), while in the case of Ti64(A-H), Ti64(A-Ca-H-W) and BG the ion exchange between the materials and the soaking solution is expected (that is of Na^+ in the first material, of Ca^{++} in the second one and of both Na^+ and Ca^{2+} in the third one).

Less common investigation techniques are used in this research to complement the traditional ones for a better understanding of the supposed mechanisms and for a comparison of the kinetics of *in vitro* hydroxyapatite precipitation. For instance, much information can be derived from the titration curves obtained by the electro-kinetic measurements of the zeta potential: the isoelectric point, presence and reactivity of surface functional groups, hydrophilicity, the zeta potential at the physiological pH and the nature of the surface charges in contact with a solution.

If we consider in a complementary way the data obtained from the zeta potential titration curves and XPS on the analyzed samples, it can be concluded that the IE point is not strictly related to abundance of functional groups on a surface, but is mainly due to the strength of their basic/acidic reactivity. It can be concluded that Ti(A-HC-H) has OH surface groups with strong basic bahaviour, while Ti64(HF-H_2O_2), BG and Ti64(A-H) have OH surface groups with an acidic behavior and strength in descending order.

On the other hand, the slope of the titration curve around the IE point, before reaching any eventual plateau, is related to surface hydrophilicity: if the material is hydrophobic, the water molecules adsorbed on it are weakly attracted by the surface and they are easily replaced by the hydroxyl (in the basic range) or hydronium ions (in the acidic range). The surface acquires a progressive higher absolute value of the zeta potential (high slope of the curve) by changing the pH. On the contrary, if the surface is hydrophilic, the water molecules are strongly adsorbed on the polar groups

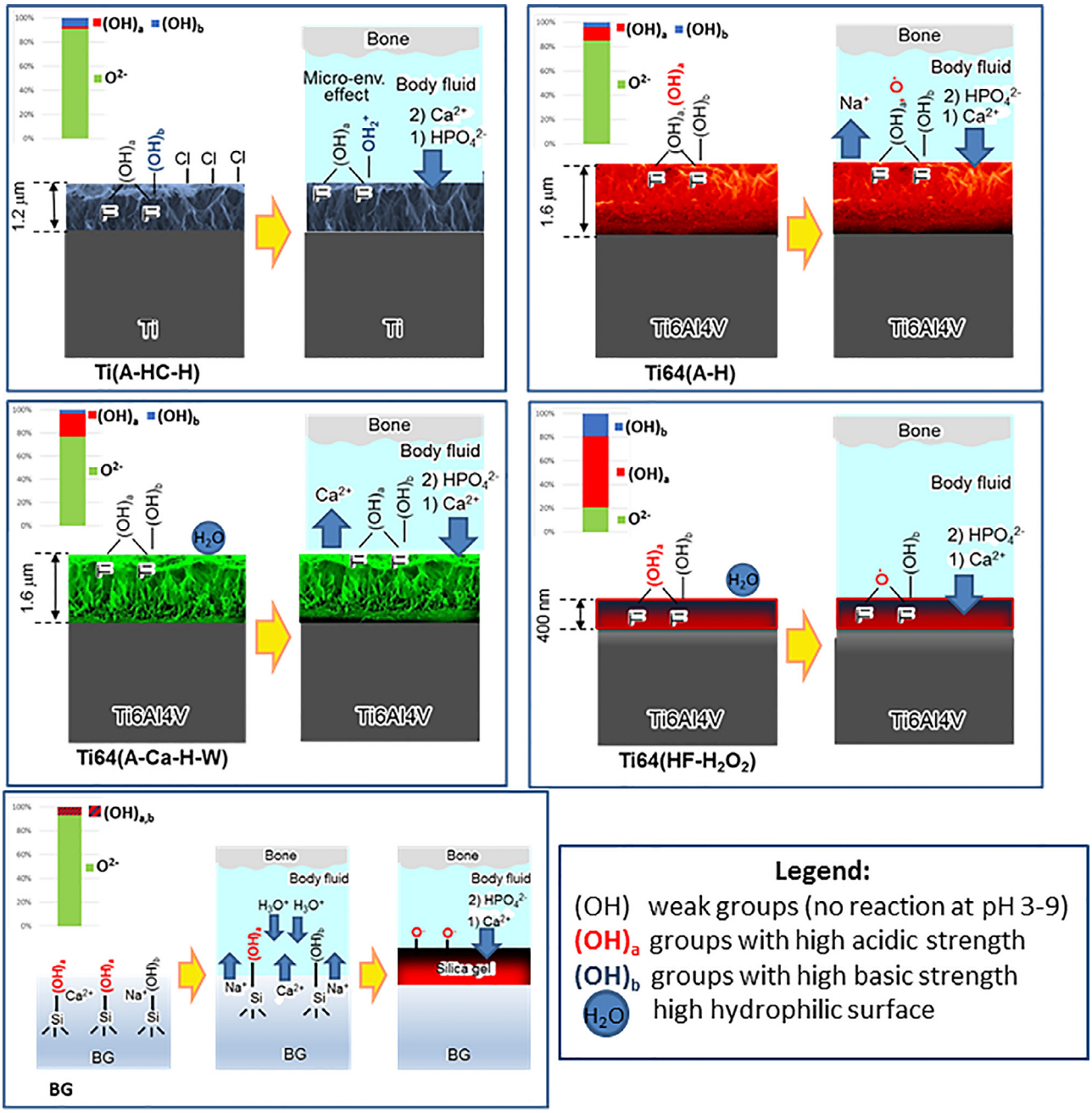

Fig. 8. Summary of the reactions and mechanisms involved in bioactivity of the investigated surface treated Ti based materials and bioactive glass.

and the OH^- and H_3O^+ ions are not adsorbed from the solution, even if they are in great concentration in the solution. In these conditions, the absolute value of the zeta potential slowly changes with the pH of the solution (slow slope of the curve). According to the explained mechanism, this technique allows the measurement of hydrophilicity as related to a "pure" chemical contribution, without the influence of any other effect such as, for instance, roughness. It can be observed that Ti64(HF-H_2O_2) and Ti64(A-Ca-H-W) are much more hydrophilic (lower slope of the curves) than the other materials: this effect is related to the total number of the OH groups on these surfaces, as confirmed by XPS and FTIR. In fact, the hydroxyl groups have a higher degree of electron bond polarization with respect to oxygen ions within the oxide. This is why they have a significant chemical shift, compared to the oxygen ions within the titanium dioxide, in the XPS signal and this is why they affect hydrophilicity: it is reasonable to assume that hydrophilicity is related to the total number of the OH groups, while their strong or weak acidic or basic strength has not an influence in this case.

All the investigated materials have a negative zeta potential at the physiological pH in the experimental conditions of the electro-kinetic test (high fluid flux, diluted KCl solution), but the chemical nature of the surface charge is different case by case, according to the obtained results. Ti64(HF-H_2O_2) and BG have a negative surface charge due to the completely dissociated OH groups with strong acidic behaviour. Ti64(A-H) has acidic OH groups of different strength, only partially dissociated at the physiological pH, while Ti64(A-Ca-H-W) has only a low number of adsorbed hydroxyl groups coming from the solution and no net surface charge due to the surface functional groups. The case of Ti(A-HC-H) is much more complex and will be discussed later.

On Ti(A-HC-H), a positive zeta potential was detected through the electro-osmosis technique, which is a measurement in a static chemical microenvironment at the physiological pH (7.0-7.4). This is because Cl^- ions that had been adsorbed on the metal surface during the HCl treatment [14] were desorbed from the surface and subsequently induced an acid environment at the vicinity of the surface. By considering the electro-kinetic and the electro-osmosis zeta potential measurements in a complementary way, it is assumed that the pH of the micro-environment become less than 5.6 (that is the IE point of this sample). The presence of a nanoporous morphology of the surface layer with a filamentous shape could contribute to the occurrence of a specific chemical micro-environment.

As described in Section 3.1, it is not surprising that a chemical microenvironment effect occurs only on Ti(A-HC-H) because on this surface there is combination of a highly porous and filamentous surface (absent on Ti64(HF-H_2O_2) and BG) together with the presence of OH groups with strong basic behavior [absent on Ti64(A-H) and Ti64(A-Ca-H-W)].

The XPS results on Ti(A-HC-H) after 30 min of soaking in SBF are well consistent with this conclusion: because of the presence of a positive surface charge locally developed during soaking in SBF, phosphate adsorption occurs in the first minutes of the soaking.

In contrast, the calcium ions are initially adsorbed on the surfaces of Ti64(A-H), Ti64(A-Ca-H-W), Ti64(HF-H_2O_2) and BG in the first 30 minutes of the soaking. In the case of Ti64(A-H), a progressive reduction of Na on the surface is observed moving from the as-prepared sample to the soaked one for 30 min according to a nucleation mechanism based on the ion exchange between the surface and the solution (as confirmed by FTIR). In the case of Ti64(A-Ca-H-W) and BG, an increasing trend of Ca is observed that is probably due to the competition between release of this ion from the surface and adsorption from the solution.

The evaluation of the kinetics of nucleation of hydroxyapatite can be performed by complementary considering the measurement of the electro-kinetic zeta potential vs time at the physiological pH during the first 30 min of the soaking, as well as XPS and FTIR chemical imaging after 30 min. Ca adsorption is much faster on BG, with formation of a continuous layer of amorphous precipitates (precursors of hydroxyapatite) and fast changing of surface charge, while it is slower on Ti64(A-H). Hydroxyapatite precursors cannot be detected after 30 min of soaking on the other samples.

Concerning the mechanism of hydroxyapatite nucleation, a significant contribution due to the protonated/deprotonated OH groups is not expected on Ti64(A-Ca-H-W): it has not basic or acidic OH groups with high strength. A contribution from the partially deprotonated OH groups can occur in the case of Ti64(A-H) and it is expected to be higher in the case of BG. On the other side, in the case of Ti64(HF-H_2O_2), the adsorption of Ca^{++} ions detected by XPS after 30 min of soaking in SBF is ascribed only to the negative charge of the surface because of deprotonation of the acidic OH groups with high strength at the physiological pH.

After nucleation, the first evolution of hydroxyapatite formation on the different surfaces can be evaluated by XPS and FTIR chemical imaging data after 1 day of soaking. On Ti(A-HC-H), Ti64(A-H), Ti64(A-Ca-H-W) and BG precipitates of calcium phosphate cover the surfaces almost completely and, as expected for the bioactive materials, hydroxyapatite is calcium deficient (theoretical Ca/P ratio = 1.67). Among these surfaces, Ti64(A-Ca-H-W) has probably slower kinetics of hydroxyapatite precipitation (FTIR and XPS data). In the case of Ti64(HF-H_2O_2), the development of calcium phosphate on the surface after 1 day of soaking is quite lower than on the other surfaces: this surface has slower kinetics of hydroxyapatite precipitation.

It can be concluded that when the precipitation mechanism is mainly based on the ion exchange with a contribution of the electrostatic mechanism (presence of OH groups with high acidic strength), it results in very fast kinetics of hydroxyapatite precipitation (the fastest is BG, with exchange of both Na^+ and Ca^{2+}, followed by Ti64(A-H), with exchange of Na^+, according to the FTIR and XPS data). Ti64(A-Ca-H-W) results to have slower kinetics of hydroxyapatite precipitation (comparison at 1 day, FTIR and XPS data) because the mechanism is based on the ion exchange of Ca^{2+} and no contribution comes from the deprotonated surface OH groups.

On the other side, the mechanism based only on the surface charge effect, such as in the case of Ti64(HF-H_2O_2), is the slowest even if abundant and strongly reactive functional groups are present on the surface. The occurrence of a micro-environment effect, in the case of Ti(A-HC-H), is able to enhance kinetics of hydroxyapatite precipitation based on a net surface charge up to be comparable with Ti64(A-Ca-H-W) (FTIR, XPS data).

Concerning the type of hydroxyapatite deposition, the presence of hydroxyapatite much closer to the biological one (type B, less crystalline and with highly carbonate degree) is earlier developed on Ti(A-HC-H) and Ti64(A-H), while Ti64(A-Ca-H-W) and BG induce precipitation of hydroxyapatite of type A-B, with higher degree of crystallinity and lower of carbonation.

After 3 days of soaking, Ti(A-HC-H), Ti64(A-H),Ti64(A-Ca-H-W) and BG show a similar thick layer of hydroxyapatite, while Ti64(HF-H_2O_2) is still at the nucleation stage.

A summary of the reactions and mechanisms involved in the hydroxyapatite precipitation on the selected materials ,as deduced from the present work, is reported in Fig. 8.

5. Conclusions

A comparison among bioactive materials with different surface features (chemistry, charge, morphology) has been performed in order to verify case by case the mechanism of nucleation and evolution of hydroxyapatite during the first 3 days of soaking.

The results suggest that the OH groups on the surface have several effects on the surface chemical behavior: a detailed description of their abundance and chemical acidic/basic reactivity can be helpful for a better understanding of surface chemistry. Abundance of OH groups mainly affects hydrophilicity of surfaces, while the isoelectric point, surface charge and ions adsorption from the solution mainly depends on the OH acidic/basic strength. Ti64(HF-H_2O_2) and BG have acidic OH groups with high strength deprotonated at the physiological pH, while Ti64(A-H) has acidic groups with a variety of different strengths (only partially deprotonated at the physiological pH) and Ti64(A-Ca-H-W) does not have a net surface charge due to the surface functional groups. Ti(A-HC-H) has basic OH groups with high strength, which are able to create, with the concurrence of a highly porous surface, a local acidic microenvironment (pH below 5.6) on the surface during soaking in SBF and a positive surface charge.

The kinetics of hydroxyapatite precipitation is faster when it is due to the ion exchange between the surface and SBF, such as in the case of Ti64(A-H), Ti64(A-Ca-H-W) and BG, with respect to a mechanism based only on electrostatic effects due to protonation/deprotonation of the surface OH groups, such as in the case of Ti64(HF-H_2O_2). In the case of Ti64(A-H) and BG, the electrostatic effect can cooperate with the ion exchange speeding up the bioactivity process. The occurrence of an acidic local environment can significantly speed up the process based on an electrostatic mechanism, such as in the case of Ti(A-HC-H).

The use of less common investigation techniques, such as the bulk zeta potential measurements (by electro-kinetic and electro-osmosis) and FTIR chemical imaging analysis, in addition to the

usual ones (FE-SEM, EDX, XPS) is useful for a more in depth comprehension of the surface chemistry and hydroxyapatite precipitation mechanism.

Declaration of Competing Interest

None.

Acknowledgements

This work was supported by MAECI: GLOBAL Project (bilateral projects Italy-Japan; Progetti di Grande Rilevanza Nazionale).

References

[1] T. Kokubo, H. Takadama, How useful is SBF in predicting in vivo bone bioactivity? Biomater 27 (2006) 2907–2915.
[2] A.A. Zadpoor, Relationship between in vitro apatite-forming ability measured using simulated body fluid and in vivo bioactivity of biomaterials, Mater Sci. Eng. C 35 (2011) 134–143.
[3] G. Kaur, O.P. Pandey, K. Singh, D. Homa, B. Scott, G. Pickrell, A review of bioactive glasses: Their structure, properties, fabrication, and apatite formation, J. Biomed. Mater. Res. Part A 102 (2014) 254–274.
[4] L.L. Hench, R.J. Splinter, W.C. Allen, T.K. Greenlee, Bonding mechanisms at the interface of ceramic prosthetic materials, J. Biomed. Mater. Res. Symp. 5 (1971) 117–141.
[5] L.L. Hench, Bioceramics, J. Am. Ceram. Soc. 81 (1998) 1705–1728.
[6] W. Cao, L.L. Hench, Bioactive materials, Ceram. Int. 22 (1996) 493–507.
[7] V. Mourino, J.P. Cattalini, A.R. Boccaccini, Metallic ions as therapeutic agents in tissue engineering scaffolds: an overview of their biological applications and strategies for new developments, J. R. Soc. Interface 9 (2012) 401–419.
[8] A. Hoppe, V. Mouriño, A.R. Boccaccini, Therapeutic inorganic ions in bioactive glasses to enhance bone formation and beyond, Biomater. Sci. 1 (2013) 254–256.
[9] F. Baino, S. Hamzehlou, S. Kargozar, Bioactive Glasses: Where Are We and Where Are We Going? J. Funct. Biomater. 9 (2018) 25.
[10] M. Miola, G. Fucale, G. Maina, E. Verné, Antibacterial and bioactive composite bone cements containing surface silver-doped glass particles, Biomed. Mater. 10 (2015) 055014.
[11] A.L. Maçon, T.B. Kim, E.M. Valliant, K. Goetschius, R.K. Brow, D.E. Day, A. Hoppe, A.R. Boccaccini, I.Y. Kim, C. Ohtsuki, T. Kokubo, A. Osaka, M. Vallet-Regí, D. Arcos, L. Fraile, A.J. Salinas, A.V. Teixeira, Y. Vueva, R.M. Almeida, M. Miola, C. Vitale-Brovarone, E. Verné, W. Höland, J.R. Jones, A unified in vitro evaluation for apatite-forming ability of bioactive glasses and their variants, J. Mater. Sci. Mater Med. 26 (2015) 115–125.
[12] T. Kokubo, S. Yamaguchi, Novel bioactive materials developed by simulated body fluid evaluation: Surface-modified Ti metal and its alloys, Acta Biomater 44 (2016) 16–30.
[13] S. Ferraris, S. Spriano, G. Pan, A. Venturello, C.L. Bianchi, R. Chiesa, M.G. Faga, G. Maina, E. Vernè, Surface modification of Ti-6Al-4V alloy for biomineralization and specific biological response: Part I, inorganic modification, J. Mater. Sci. Mater. Med. 22 (2011) 533–545.
[14] D.K. Pattanayak, S. Yamaguchi, T. Matsushita, T. Kokubo, Effect of heat treatments on apatite-forming ability of NaOH- and HCl-treated titanium metal, J. Mater Sci: Mater Med: 22 (2011) 273–278.
[15] S. Yamaguchi, .K Akeda, K. Murata, N. Takegami, M. Goto, A. Sudo, T. Matsushita, T. Kokubo, Chemical and Heat Treatments for Inducing Bone-Bonding Ability of Ti-6Al-4V Pedicle Screw, Key Eng Mater 631 (2015) 225–230.
[16] K. Sieradzka, J. Domaradzki, E. Prociów, M. Mazur, M. Łapiński, Properties of nanocrystalline TiO2:V thin films as a transparent semiconducting oxides, Acta Phys. Pol. A 116 (2009) S-33–S-35.
[17] P.S Archana, R. Jose, T.M. Jin, C. Vijila, M.M. Yusoff, S. Ramakrishnaw, Structural and Electrical Properties of Nb-Doped Anatase TiO2 Nanowires by Electrospinning, J. Am. Ceram. Soc. 93 (2010) 4096–4102.
[18] A. Grunenwald, C. Keyser, A-M. Sautereau, E. Crubézy, B. Ludes, C. Drouet, Revisiting carbonate quantification in apatite (bio)minerals: a validated FTIR methodology, J. Arch. Sci. 49 (2014) 134–141.
[19] C. Wu, K. Tu, J. Deng, Y. Lo, C. Wu, Markedly Enhanced surface hydroxyl groups of TiO2 nanoparticles with superior water-dispersibility for photocatalysis, Materials 10 (2017) 566–581.
[20] Y. Hong, M. Yu, J. Lin, K. Cheng, W. Weng, H. Wang, Surface hydroxyl groups direct cellular response on amorphous and anatase TiO2 nanodots, Coll. Surf. B: Bioint. 123 (2014) 68–74.
[21] M. Cerruti, C.L. Bianchi, F. Bonino, A. Damin, A. Perardi, C. Morterra, Surface Modifications of Bioglass Immersed in TRIS-Buffered Solution. A Multitechnical Spectroscopic Study, J. Phys. Chem. B 109 (2005) 14496–14505.
[22] W. Xia, C. Lindahl, J. Lausmaa, H. Engqvist, Biomimetic hydroxyapatite deposition on titanium oxide surfaces for biomedical application, Adv. Biomimet. (2011) Prof. Marko Cavrak (Ed.), ISBN: 978-953-307-191-6.
[23] H.A. Shalaby, A.M. Hashem, N.A. Badr, M.M. Shoeib, M.G. Khafagy, Preparation of ordered nano-titania arrays and electrodeposition of nano- hydroxyapatite crystals on ti6al%-4%v dental implant surfaces, J. Am. Sci. 7 (2011) 574–584.
[24] M. Ladan, W.J. Basirun, S.N. Kazi, F.A. Rahman, Corrosion protection of AISI 1018 steel using Co-doped TiO2/polypirrole nanocomposites in 3.5% NaCl solution, Mat. Chem. Phys. 192 (2017) 361–373.
[25] B. Simović, A. Dapčević, J. Zdravković, N. Tasić, S. Kovač, J. Krstić, G. Branković, From titania to titanates: Phase and morphological transition in less alkaline medium under mild conditions, J. Alloys Compounds 781 (2019) 810–819.
[26] A Sroka -Bartnicka, L Borkowski, G Ginalska, A Slosarczyk, G Kazarian S, Structural transformation of synthetic hydroxyapatite under simulated *in vivo* conditions with ATR-FTIR spectroscopic imaging, Spec. Acta A: Mol. Biomol. Spec. 171 (2017) 155–161.
[27] T.T. Demirtas, G. Kaynak, M. Gümüşderelioğlu, Bone-like hydroxyapatite precipitated from 10×SBF-like solution by microwave irradiation, Mat. Sci. Eng. C 49 (2015) 713–1719.